The Cryosphere Discuss., https://doi.org/10.5194/tc-2017-260
Manuscript under review for journal The Cryosphere
Discussion started: 5 December 2017
© Author(s) 2017. CC BY 4.0 License.

The Cryosphere Discussions
Open Access
EGU

Estimation of Arctic Land-Fast Ice Cover based on SENTINEL-1 SAR Imagery

Juha Karvonen[1]

[1]Finnish Meteorological Institute, PB 503, FI-00101, Helsinki, Finland

Correspondence to: Juha Karvonen (juha.karvonen@fmi.fi)

Abstract. Here we present a method for estimating the land-fast ice (LFI) extent from SENTINEL-1 SAR mosaics over an Arctic study area ove Kara and Barents Seas. The method is based on temporal cross-correlation between adjacent day SAR mosaics. The results are compared to the LFI of the Russian Arctic-Antarctic Research Institute (AARI) ice charts. A LFI time series covering the time period from October 2015 to the end of August 2017 computed using the presented methodology is provided on our ftp server. The time series will be extended twice annually.

1 Introduction

Land-fast ice (also known as shore-fast ice, or shortly as fast ice), here denoted by LFI, is sea ice that is attached to the coastline, to the sea floor along shallow areas or to grounded icebergs (WMO , 2015; Weeks , 2010; Lepparanta , 2011). LFI may either grow in place from the sea water or by freezing drifting ice to the shore (WMO , 2015). LFI does not move with currents and winds. Fast ice zone is typically seasonal and depends on ice thickness, topography of the sea floor and islands (Lepparanta , 2011). On average the fast ice edge is located in the water depth of 10-25 m (Zubov , 1945; **?**; Mahoney et al. , 2007). However, there exists seasonal and inter-annual variability. LFI area covers approximately 13% of the Northern Hemisphere area of sea ice coverage (Yu et al. , 2014) and thus represents an essential fraction of the Arctic sea ice. LFI range from coast varies from a few meters to several hundreds of kilometers (WMO , 2015). For practical LFI detection we need to fix some criteria to detect the LFI areas. In (Mahoney et al. , 2005) two criteria have been used for LFI: the ice is contiguous with land and it lacks detectable motion for approximately 20 days. In our method presented here we have used quite similar criteria.

Long-term changes have been found in the LFI regime. The trend seems to be toward reducing LFI area (Divine et al. , 2003; Yu et al. , 2014), later formation and earlier disappearance (Mahoney et al. , 2014) and reduction of the LFI thickness (Polyakov et al. , 2003, 2012). Although LFI zone only covers a relatively small fraction of overall Arctic sea ice extent, it has particular importance for the coastal systems, e.g. by defining the location of polynyas (Seluyzhenok et al. , 2015). These facts make monitoring of the LFI zone important also as a climate change indicator. Also in the fast ice zone only thermodynamic ice modelling is necessary as the modelled dynamic part can be omitted. This will increase the reliability of the ice modelling, assuming that the LFI areas can reliably be located, over the LFI areas as the uncertainties originating from the ice dynamics will be excluded. The proposed method has been used and will be used for creating daily time series of the Kara and Barents Sea LFI extent in high-resolution complementing the existing LFI time series.

The Cryosphere Discuss., https://doi.org/10.5194/tc-2017-260
Manuscript under review for journal The Cryosphere
Discussion started: 5 December 2017
© Author(s) 2017. CC BY 4.0 License.

LFI detection based on different techniques and different instruments have been proposed. Passive microwave (PM) data is widely used for determining sea ice motion, e.g. in (Agnew et al. , 1997; Kwok et al. , 1998), but because of their low spatial resolution (5-50 km) it has not been used much for fast ice detection (Fraser et al. , 2011). Some examples of usig PM data for LFI estimation exist e.g. temporal correlation median of AMSR-E imagery was used for LFI detection in (Seluyzhenok , 2011). High resolution near-infrared imagery from Landsat I and II have been used for identification Alaska's LFI as sea ice contiguous with the coast (Barry et al. , 1979; Stringer et al. , 1978, 1980). A method for estimating LFI using cloudless specroradiometer (MODIS) data was proposed in (Fraser et al. , 2011), more specifically using a 20-day composite of MODIS imagery of eastern Antarctic coast supported by AMSR-E ASI sea ice concentration in the case on unreliable (possibly cloudy) MODIS composites. In (Kim et al. , 2015) machine learning (Random Forest algorithm) using data from multiple instruments (AMSR-E brightness temperature, MODIS ice sufrace temperature (IST) and SSMI ice velocity) were applied for LFI detection. In the study ice velocity and IST proved to be the most significant variables for LFI detection.

Also different methods utilizing SAR imagery for LFI detection have been proposed. A significant advantage of using SAR imagery is their high resolution, typically from tens to a few hundreds of meters. In (Antonova , 1997) the areas of static ice were determined manually from consecutive SAR images (time series). In (Mahoney et al. , 2004, 2005) LFI is detected based on SAR mosaic edges and their orientation (gradients) and their temporal differencies. The bottom fast ice zone can be identified based on the SAR backscatter (Eicken et al. , 2005; Solomon et al. , 2003) as if there is no ice-water interface the dielectric contrast at the bottom is significantly reduced. Ice drift can be derived from multi-temporal SAR image pairs over the same area. Such SAR ice drift detection algorithms are typically based on temporal cross-correlation (Fily and Rothrock , 1987), phase-correlation (Thomas et al. , 2008) or optical flow (Sun , 1996). From these ice drift estimates it is possible to derive the static ice areas which can be interpreted as LFI, assuming there is long-enough time series of ice drift at a certain location. Also SAR interferometry can be used for LFI detection, see e.g. (Marbouti et al. , 2017), as the phase difference is random for drift ice and coherent for the static ice fields. In (Karvonen , 2012) the cumulative Baltic sea ice drift was used for locating the Baltic sea LFI by indicating the areas where no ice motion has occurred within a given, long-enough time period. In (Karvonen , 2014) directly applied temporal cross-correlation minimum was used to locate the fast ice to aid sea ice concentration estimation.

2 Study Area, Data Sets and Pre-Processing

2.1 Study area

The study area is located in the Kara and Barents Seas and the area is shown in Fig. 1. The polar stereographic projection we use in this paper has a mid-longitude of 55E, reference latitude of 70N (latitude of the correct scale) and the datum is WGS84. The upper left (UL) and lower right (LR) coordinates of the area are (northing and easting in meters): UL=(-700000,-1100000) and LR=(-2550000,1100000).

The Cryosphere Discuss., https://doi.org/10.5194/tc-2017-260
Manuscript under review for journal The Cryosphere
Discussion started: 5 December 2017
© Author(s) 2017. CC BY 4.0 License.

2.2 Russian Ice Charts

The Russian Arctic ice charts are provided weekly by AARI on their web page (the English version on http://www.aari.ru/odata/_d0015.php They are provided as thematic maps in polar stereographic projection with the mid-longitude of 90°E. We re-reprojected these ice charts to our polar stereographic projection and extracted the LFI areas based on the colormap. An example of the Russian ice chart of March 8 2016 is shown in Fig. 2. We used LFI from 35 AARI ice charts from the period from November 3 2015 to July 5 2016 as reference LFI data for evaluating the proposed algorithm.

2.3 SENTINEL-1 imagery, SAR Mosaic and their processing

We have used all the available C-band SENTINEL-1 dual-polarized Extra Wide (EW) swath mode level 1 Ground Range Detected Medium resolution (GRDM) data with the HH/HV polarization channels over the study area. The SAR data are publicly available through the Copernicus Science Hub (https://scihub.copernicus.eu/). The imagery were preprocessed by applying an incidence angle correction for the HH channel and a combined incidence angle and noise floor correction for the HV channel, for details of this process, see (Karvonen , 2017). After corrections the image data were rectified to the polar stereographic projection introduced in Section 2.1. After rectification the imagery were still down-sampled to 500 m resolution and finally the daily mosaics were constructed by overlaying the newer images over the older ones such that at each mosaic grid cell (pixel) the newest SAR data is available. Separate mosaics for HH and HV channels were constructed. A land mask based on the GSHHG coastline data set (Wessel and Smith , 1996) is applied to the mosaics to exclude land areas from LFI computation. Dual-polarized EW mode SENTINEL-1 data are systematically acquired over the European Arctic and Greenland waters. In the upper right corner of our study area there is no dual-polarized SENTINEL-1 EW mode data available. This can be seen as a black area in Fig. 3 where the HH and HV SENTINEL-1 SAR mosaics of March 8, 2016 are shown.

3 Methodology for estimation of land fast ice areas

The fast ice estimation is based on the temporal average of cross-correlation of adjacent day SAR mosaics. The same processing is performed for both HH and HV polarization channel images. The processing for the HH channel is illustrated in the block diagram of Fig. 4. The processing for the HV channel is similar except that a different threshold T_{HV} instead of T_{HH} is applied.

To fasten the computation and to exclude areas where LFI does not appear we produced a mask indicating the potential LFI areas as areas which are 100 km or less from the coast (including islands). This is a very simple approach and in some other areas a more sophisticated mask, taking into account the bathymetry, e.g. using a given distance from the depth of 25 m, may be needed. The mask applied here is shown in Fig. 5.

For the areas defined by the mask, i,e, white areas in Fig. 4 the temporal cross-correlation (TCC) between two adjacent days' mosaics is computed, using a circle-shaped window with a radius of 3 mosaic pixels in the computations. The areas where TCC is one are excluded from the average computation as they represent the areas where the mosaic has not updated

The Cryosphere Discuss., https://doi.org/10.5194/tc-2017-260
Manuscript under review for journal The Cryosphere
Discussion started: 5 December 2017
© Author(s) 2017. CC BY 4.0 License.

since the previous day. For SAR data from two different SAR images TCC is in practice always less than zero because of the speckle present in all radar imagery. TCC is computed for both SAR HH and HV channels. The initial decision is made based on thresholding of TCC: the grid cell is considered as possible LFI if $TCC_{HH} > 0.19$ and $TCC_{HV} > 0.15$ and they are in the area defined by the mask (distance from land less than 100 km). Additionally we perform a morphological opening operation (i.e. erosion followed by dilation) by a disk with a radius of two pixels to remove narrow elongated high TCC segments (which are typically due to boundaries of SAR frames over open water, where the incidence angle correction often fails because of varying wave conditions) and small single areas which are also typically errors caused by small singular targets (e.g. big ships or icebergs). We still additionally applied removal of small LFI segments. The small segment filtering performs removal of segment smaller than a given threshold value (T_S), we have used T_s = 100 pixels, corresponding to an area of 25 km^2. This efficiently reduces the number small erronous segments due to SAR artefacts. After the small segment elimination we get the product referred here as method A or shortly FMI-A.

To further improve the estimation from FMI-A we still additionally perform a two-week (14 days) temporal logical and operation of the fourteen adjacent day FMI-A products. This result is referred here as method B (FMI-B) in this context.

4 Results

We first computed the reults for a test data set over a period ranging from November 2015 to early July 2016, and compared the results with the weekely AARI ice charts. The comparison was pixel-based and it was performed between the daily LFI product and the corresponding AARI LFI of the same date (ice chart issuing date). Totally we used 35 weekly AARI ice charts in the comparison (period from November 3 2015 to July 5 2016). The results of the comparison can be seen in Table 1. The first column of the table provides the AARI ice chart (IC) LFI area, the second column provides the LFI area provided by the FMI algorithms over the ice chart LFI area, the third column provides the ice chart LFI area over areas where no LFI was detected by the SAR algorithm, and finally the fourth column provides the LFI area given by the SAR algorithm over the area of no LFI according to the ice charts. The correspondence was quite good even though there also exist differencies. Part of these differences are due to the more precise LFI detection of the automated algorithms. It is also dependent on the definition of fast ice, our automated algorithms locate the ice areas which has been static over a given time. An example of the AARI ice chart LFI and the FMI-A and FMI-B LFI of March 8, 2016 is shown in Fig. **??**.

In general the same LFI areas as in the AARI ice charts were identified by both FMI-A and FMI-B. However, FMI-A detected more LFI than present in the AARI ice charts and FMI-B. Also in some coastal areas the FMI algorithms detected more LFI than present in the AARI ice charts. This is at least partly due to the inaccuracies of the land mask and possible inclusion of some land pixels. We also provide an example of combining the results of AARI ice charts and two FMI methods into a single false color RGB image with AARI LFI on the red color channel, FMI-A on the green color channel and FMI-B on the blue color channel, This example is shown in Fig. 7.

We also computed and compared the weekly LFI extent over the whole study using FMI-A, FMI-B and the 35 weekly AARI ice charts over our study area. These results can be seen in Fig. 8. We can see that FMI-B LFI extent is closer to the AARI LFI

© Author(s) 2017. CC BY 4.0 License.

extent. Additionally we also computed the ice extent for the whole current time series period from October 15 2015 to the end of August 2017. This time series is shown in Fig. 9. It should be noted that according to the figure there also exist some LFI during the summer. This seems to be a constant value and due to the erronous detection close to the coasts, probably due to inaccuracies in the land mask. In principle these areas could be filtered out e.g. by entending the land mask over these areas. However, we have not done this in this version of the product but it can easily be done by the user.

According to the time series the seasonal LFI extent maximum over our study area was some larger in 2017 (January-April) reaching about 50000 km^2. The duration of the maximum extent (with minor variation) was approximately the same for both the studied winters (2016 and 2017), but in 2017 LFI disappeared faster.

5 Discussion and Conclusions

We have developrd an algorithm for detecting LFI over a test area in the Kara and Barents seas using daily SENTINEL-1 dual-polarized SAR mosaics. Both SAR channels (HH and HV) have been used jointly for reliably estimating the LFI area. We have generated daily LFI area estimates for a period ranging from October 2015 to August 2017. The data were also evaluated against weekly Russian AARI ice charts and the correspondence was rather good. According to this study the algorithm is suitable for operational LFI monitoring based on C-band SAR imagery.

Use of temporal average and temporal median in the algorithm produced quite similar results and because of its faster computation we have here applied temporal average instead of temporal median (requiring sorting of the samples). The execution times on a single CPU-core (Intel Xeon 2.5GHz) with a sufficient amount of RAM memory were reasonable also for operational purposes: computation of LFI extent for one daily SAR mosaic takes just some minutes. As the computation can easily be parallelized, LFI extent estimation e.g. for the whole Arctic or Antarctic areas can easily be performed in a reasonable time by dividing the workload to multiple CPU cores.

An LFI product covering the whole Arctic based on SENTINEL-1 is also possible. There is one limitation related to the SENTINEL-1 acquisition mode: over most of the Arctic SENTINEL-1 is acquiring EW mode HH polarization only and the dual-polarized data are acquired only over the European Arctic and Greenland areas. However, we believe that even HH channel data alone is sufficent for estimating the LFI extent, even though combining the two polarization channels would increase the reliability of the product to some extent.

According to the results shown here there seems to be LFI even during the summer months. This is naturally not true in the study area, and those areas indicated as LFI by the algorithm are typically areas very close to the coastline. These falsely detected LFI areas are also the same for the both the summers included in our time series. These areas are because the land mask does not fit perfectly and some land or mixed pixels are included in the computation. These could be excluded by extending the land mask by these falsely identified summer LFI areas. However, we have not done this and it should be done by the data users when seen necessary.

The Cryosphere Discuss., https://doi.org/10.5194/tc-2017-260
Manuscript under review for journal The Cryosphere
Discussion started: 5 December 2017
© Author(s) 2017. CC BY 4.0 License.

We have plans to continue computing a time series of daily LFI over our study area and update the LFI data set twice annually, once in spring and once in autumn. The data will be provided to interested parties through the FMI ftp in GeoTIFF (thematic map) and NetCDF (numeric data) formats.

Additional conditions could be included for an improved algorithm. For example taking into account the bathymetry and also requiring that the detected LFI areas are adjacent (i.e. the LFI segment has a at least some common boundary with land pixels) to land. This kind of additional conditions have not been applied in the algorithms proposed here, but may be needed in some other areas.

© Author(s) 2017. CC BY 4.0 License.

References

Agnew, T.A., H. Le, T. Hirose, Estimation of large scale sea ice motion from SSM/I 85.5 GHz imagery, Annals of Glaciology, 25, 305-311, 1997.

Sofya Antonova, Spatial and temporal variability of the fast ice in the Russian Arctic Master Thesis, State University of St. Petersburg, Russia and University of Hamburg, Germany, St. Petersburg, 2011.

Barry, R. G., R. E. Moritz, J. C. Rogers, The fast ice regimes of the Beaufort and Chucksi Sea coasts, Alaska, Cold Regions Science and Technology, v.1, n. 2, pp. 129-152.

Divine, D., R. Korsnes, A. Makshtas, Variability and climate sensitivity of fast ice extent in the north-eastern Kara sea, Polar Res., v. 22, n. 1, pp. 27–34, 2003.

Divine, D. V., R. Korsnes, A. P. Makshtas, Temporal and spatial variation of shore-fast ice in the Kara Sea, Cont. Shelf Res., v. 24, n. 15, pp. 1717–1736, doi:10.1016/j.csr.2004.05.010, 2004.

Eicken, H., Dmitrenko, I., Tyshko, K., Darovskikh, A., Dierking, W., Blahak, U., Groves, J.; Kassens, H., Zonation of the Laptev Sea landfast ice cover and its importance in a frozen estuary, Global and Planetary Change, v. 48, n. 1-3, pp. 55-83, 2005.

Fily, M. and Rothrock, D. A.: Sea ice tracking by nested correlations, IEEE T. Geosci. Remote, GE-25, 5, 570–580, 1987

Fraser, A.D., Massom, R.A., Michael, K.J., Generation of high-resolution East Antarctic landfast sea-ice maps from cloud-free MODIS satellite composite imagery, Remote Sensing of Environment, 2011.

J. Karvonen Operational SAR-based sea ice drift monitoring over the Baltic Sea, Ocean Science, v. 8, pp. 473-483, (http://www.ocean-sci.net/8/473/2012/os-8-473-2012.html) 2012

J. Karvonen, Baltic Sea Ice Concentration Estimation Based on C-Band Dual-Polarized SAR Data, IEEE Trans. on Geoscience and Remote Sensing, v. 52, n. 9, pp. 5558–5566, 2014.

J. Karvonen, Baltic Sea Ice Concentration Estimation Using SENTINEL-1 SAR and AMSR2 Microwave Radiometer Data, IEEE Transactions on Geoscience and Remote Sensing, v. 55, n. 5, pp. 2871-2883, DOI: 10.1109/TGRS.2017.2655567, 2017.

Miae Kim, Jungho Im, Hyangsun Han, Jinwoo Kim, Sanggyun Lee, Minso Shin, Landfast sea ice monitoring using multisensor fusion in the Antarctic GIScience & Remote Sensing, Volume 52, n. 2, Pages 239-256, 2015.

Kwok, R., A. Schweiger, D.A. Rothrock , S. Pang, C. Kottmeier, Sea ice motion from satellite passive microwave imagery assess with ERS SAR and buoy motions. J. Geophy. Res., 103, C4, 8191-8214, 1998.

Lepparanta, M. ,The Drift of Sea Ice, 2nd ed., Springer-Verlag, Berlin-Heidelberg, Germany, 2011.

Mahoney, A., Eicken, H., Graves, A., Shapiro, L., and Cotter, P.. Landfast sea ice extent and variability in the Alaskan Arctic derived from SAR imagery. IEEE International Geoscience and Remote Sensing Symposium Proceedings (IGARSS'04), Vol. 3. (pp. 2146-2149), 2004.

Mahoney, A., H. Eicken, L. Shapiro, A. Graves, Defining and locating the seaward landfast ice edge in northern Alaska, 18th International Conference on Port and Ocean Engineering under Arctic Conditions, Potsdam, N.Y., June 26-30, 2005.

Mahoney, A., H. Eicken, A. G. Gaylord, L. Shapiro, Alaska landfast sea ice: Links with bathymetry and atmospheric circulation, J. Geophys. Res., v. 112, C02001, doi:10.1029/2006JC003559, 2007.

Mahoney, A. R., H. Eicken, A. G. Gaylord, R. Gens, Landfast sea ice extent in the Chukchi and Beaufort seas: The annual cycle and decadal variability, Cold Reg. Sci. Technol., v. 103, pp. 41–56, doi:10.1016/j.coldregions.2014.03.003, 2014.

Marbouti, M. J. Praks, O. Antropov, E. Rinne, M. Lepparanta, A Study of Landfast Ice with Sentinel-1 Repeat-Pass Interferometry over the Baltic Sea, Remote Sensing, v. 9, n. 8, 833; doi:10.3390/rs9080833

© Author(s) 2017. CC BY 4.0 License.

Polyakov, I. V., G. V. Alekseev, R. V. Bekryaev, U. S. Bhatt, R. Colony, M. A. Johnson, V. P. Karklin, D. Walsh, A. V. Yulin, Long-term ice variability in Arctic marginal seas, J. Clim., v. 16, n. 12, pp. 2078–2085, doi:10.1175/1520-0442(2003)016<2078:Liviam>2.0.CO;2, 2003.

Polyakov, I. V., J. E. Walsh, R. Kwok, Recent changes of Arctic multiyear sea ice coverage and the likely causes, Bull. Am. Meteorol. Soc., v. 93, n. 2, pp. 145–151, doi:10.1175/Bams-D-11-00070.1, 2012.

Selyuzhenok, V., Validation of the satellite-based landfast ice mapping, Master Thesis, State University of St. Petersburg, Russia and University of Hamburg, Germany, St. Petersburg, 2011.

Seluyzhenok, V., T. Krumpen, A. Mahoney, M. Janout, R. Gerdes, Seasonal and interannual variability of fast ice extent in the southeastern Laptev Sea between 1999 and 2013, Journal of Geophysical Research, v. 120, n. 13, pp. 7791-7805, doi: 10.1002/2015JC011135, 2015.

Solomon, S. M., G. Manson, D. Monita, T. Hirose, D. Power, Synthetic Aperture Radar Remote Sensing of Bottom Fast ice in the MacKenzie Delta Region, Northwest Territories, Canada, American Geophysical Union, Spring Meeting, 2004.

Stringer, W.J., S.A. Barrett, L. Schreurs, Morphology of the Beaufort, Chukchi and Bering Seas nearshore ice conditions by means of satellite and aerial remote sensing: final report, Research unit 257, Geophysical Institute, University of Alaska Fairbanks, Fairbanks, Alaska, 1978.

Stringer, W. J., S. A. Barrett, L. K. Schreurs, Nearshore Ice Conditions and Hazards in the Beaufort, Chukchi and Bering Seas, Geophysical Institute, University of Alaska, Fairbanks, AK, USA, 1980.

Sun, Y., Automatic ice motion retrieval from ERS-1 SAR images using the optical flow method, Int. J. Remote Sens., v. 17, pp. 2059–2087, 1996.

Thomas, M., Geiger, C. A., and Kambhamettu, C., High resolution (400 m) motion characterization of sea ice using ERS-1 SAR imagery, Cold Regions Science and Technology, 52, 207–223, 2008.

Weeks, W. F., On Sea Ice, University of Alaska Press, Fairbanks, Alaska, USA, ISBN 978-1-60223-101-6, 2010.

Wessel, P., W. H. F. Smith, A Global Self-consistent, Hierarchical, High-resolution Shoreline Database, J. Geophys. Res., v. 101, pp. 8741-8743, 1996.

WMO, WMO Sea-Ice Nomenclature, World Meteorological Organization, No.259, available online: http://www.jcomm.info/index.php?option=com_oe&task=viewDocumentRecord&docID=14598, 2015.

Yu, Y. L., H. Stern, C. Fowler, F. Fetterer, J. Maslanik, Interannual variability of Arctic landfast ice between 1976 and 2007, J. Clim., v. 27, n. 1, pp. 227–243, doi:10.1175/JCLI-D-13-00178.1, 2014.

Zubov, N. N. (1945), Arctic Sea Ice (in Russian), Izd. Glavsevmorputi, Moscow, 1945.

The Cryosphere Discuss., https://doi.org/10.5194/tc-2017-260
Manuscript under review for journal The Cryosphere
Discussion started: 5 December 2017
© Author(s) 2017. CC BY 4.0 License.

Table 1. Comparison by numbers. The values in parentheses are standard deviations in percentage points.

Method	A(IC)	A(SAR|IC)	A(IC| ∼SAR)	A(SAR| ∼IC)
FMI-A (km^2)	33969	27719	6250	31387
(%)	100	81.6 (17.2)	18.4 (17.2)	92.4 (42.3)
FMI-B (km^2)	33969	23303	10666	12738
(%)	100	68.6 (21.9)	31.4 (21.9)	37.5 (11.4)

The Cryosphere Discuss., https://doi.org/10.5194/tc-2017-260
Manuscript under review for journal The Cryosphere
Discussion started: 5 December 2017
© Author(s) 2017. CC BY 4.0 License.

Figure Captions

Figure 1. The study area in polar stereographic projection.

Figure 2. AARI ice chart of March 8, 2016. ©AARI.

Figure 3. SAR mosaics of March 8, 2016, HH mosaic (left panel) and HV mosaic (right panel). The land areas, based on our land mask, and areas of no data are black in the mosaics.

Figure 4. Block diagram of the LFI detection for SENTINEL-1 HH polarization channel.

Figure 5. Mask used to locate the areas where LFI is searched. White areas are the search area, gray areas are land.

Figure 6. ARI ice chart of March 8, 2016, translated to the polar stereographic projection used in this study, LFI based on the AARI ice chart (black areas), LFI based on the FMI method, and LFI based on the FMI method with additional temporal filtering.

Figure 7. A false color image of March 8, 2016, combining the products in comparison. In the False color image Red=AARI LFI, Green=FMI-A LFI and Blue=FMI-B LFI. In the white areas all the three LFI estimates agree.

Figure 8. Time series of the weekly (from Nov 3 2015 until July 5 2016) LFI extent over the study according to FMI-A, FMI-B and AARI ice charts.

Figure 9. A LFI area times series of the whole study period from October 15 2015 to August 30 2017, using the FMI-B algorithm.

The Cryosphere Discuss., https://doi.org/10.5194/tc-2017-260
Manuscript under review for journal The Cryosphere
Discussion started: 5 December 2017
© Author(s) 2017. CC BY 4.0 License.

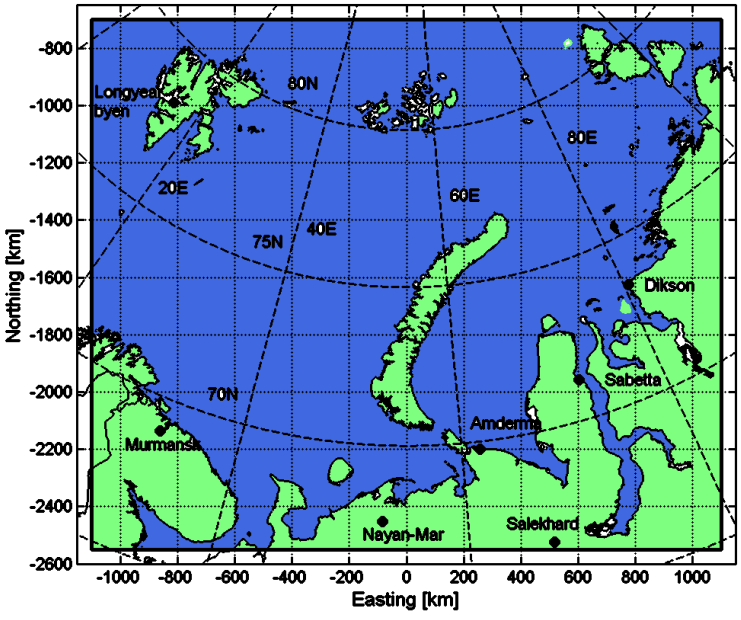

Figure 1. The study area in polar stereographic projection.

The Cryosphere Discuss., https://doi.org/10.5194/tc-2017-260
Manuscript under review for journal The Cryosphere
Discussion started: 5 December 2017
© Author(s) 2017. CC BY 4.0 License.

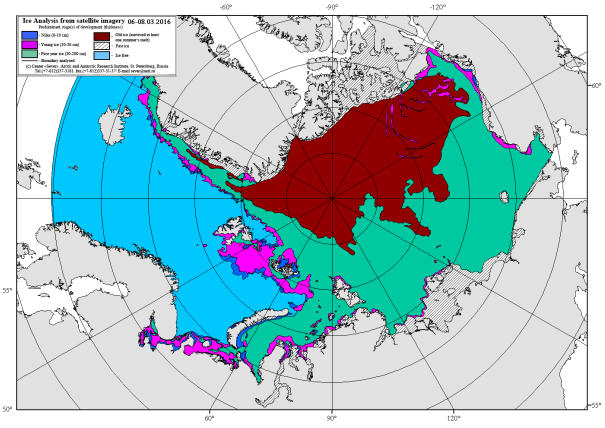

Figure 2. AARI ice chart of March 8, 2016. ©AARI.

The Cryosphere Discuss., https://doi.org/10.5194/tc-2017-260
Manuscript under review for journal The Cryosphere
Discussion started: 5 December 2017
© Author(s) 2017. CC BY 4.0 License.

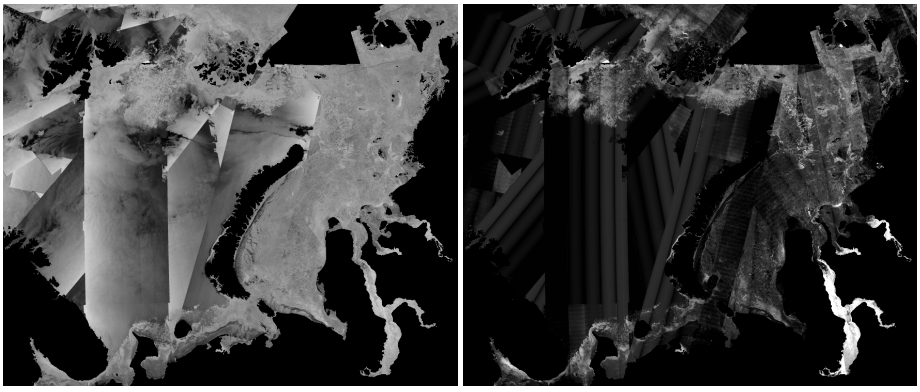

Figure 3. SAR mosaics of March 8, 2016, HH mosaic (left panel) and HV mosaic (right panel). The land areas, based on our land mask, and areas of no data are black in the mosaics.

The Cryosphere Discuss., https://doi.org/10.5194/tc-2017-260
Manuscript under review for journal The Cryosphere
Discussion started: 5 December 2017
© Author(s) 2017. CC BY 4.0 License.

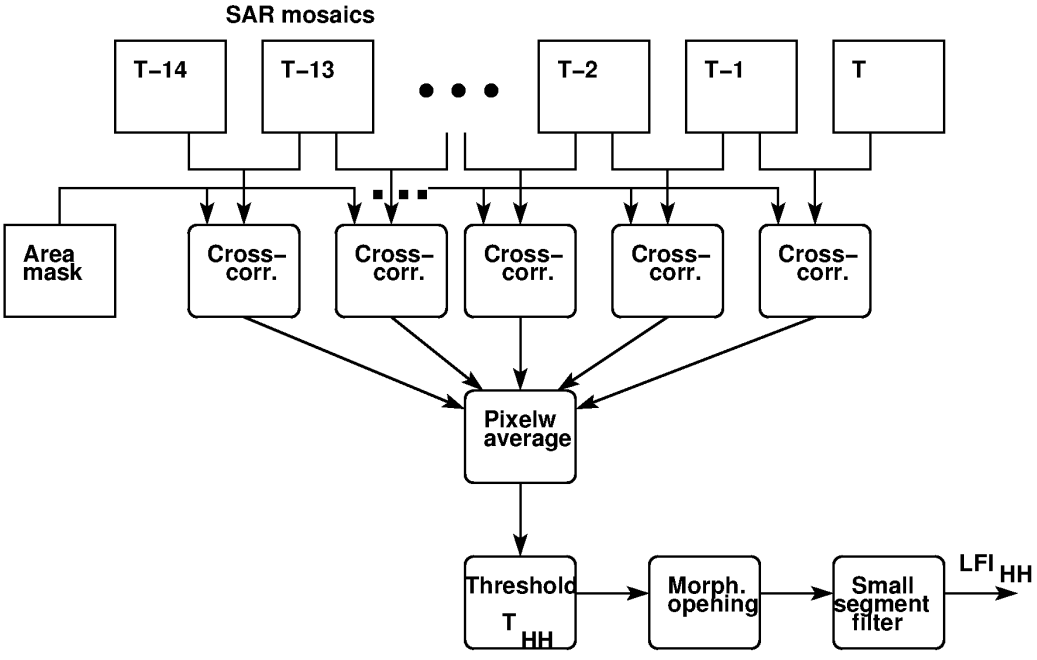

Figure 4. Block diagram of the LFI detection for SENTINEL-1 HH polarization channel.

The Cryosphere Discuss., https://doi.org/10.5194/tc-2017-260
Manuscript under review for journal The Cryosphere
Discussion started: 5 December 2017
© Author(s) 2017. CC BY 4.0 License.

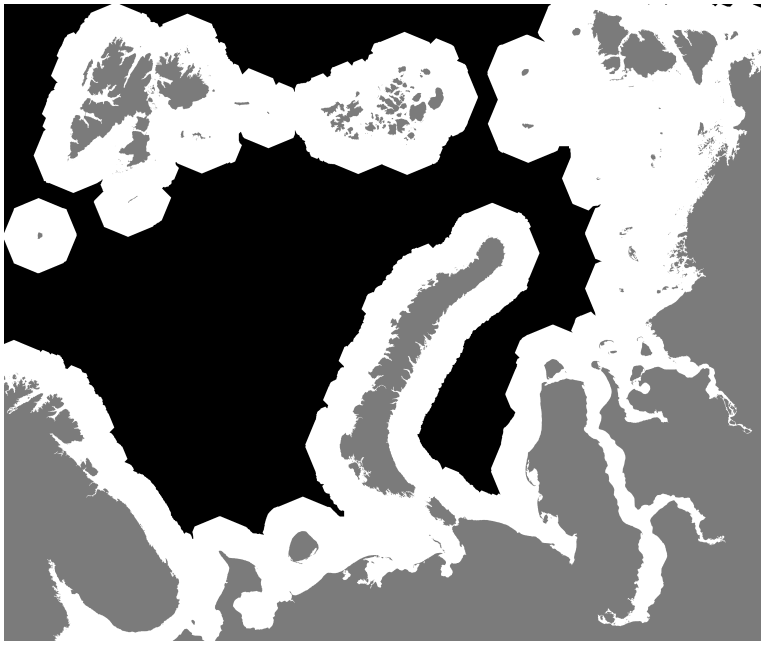

Figure 5. Mask used to locate the areas where LFI is searched. White areas are the search area, gray areas are land.

The Cryosphere Discuss., https://doi.org/10.5194/tc-2017-260
Manuscript under review for journal The Cryosphere
Discussion started: 5 December 2017
© Author(s) 2017. CC BY 4.0 License.

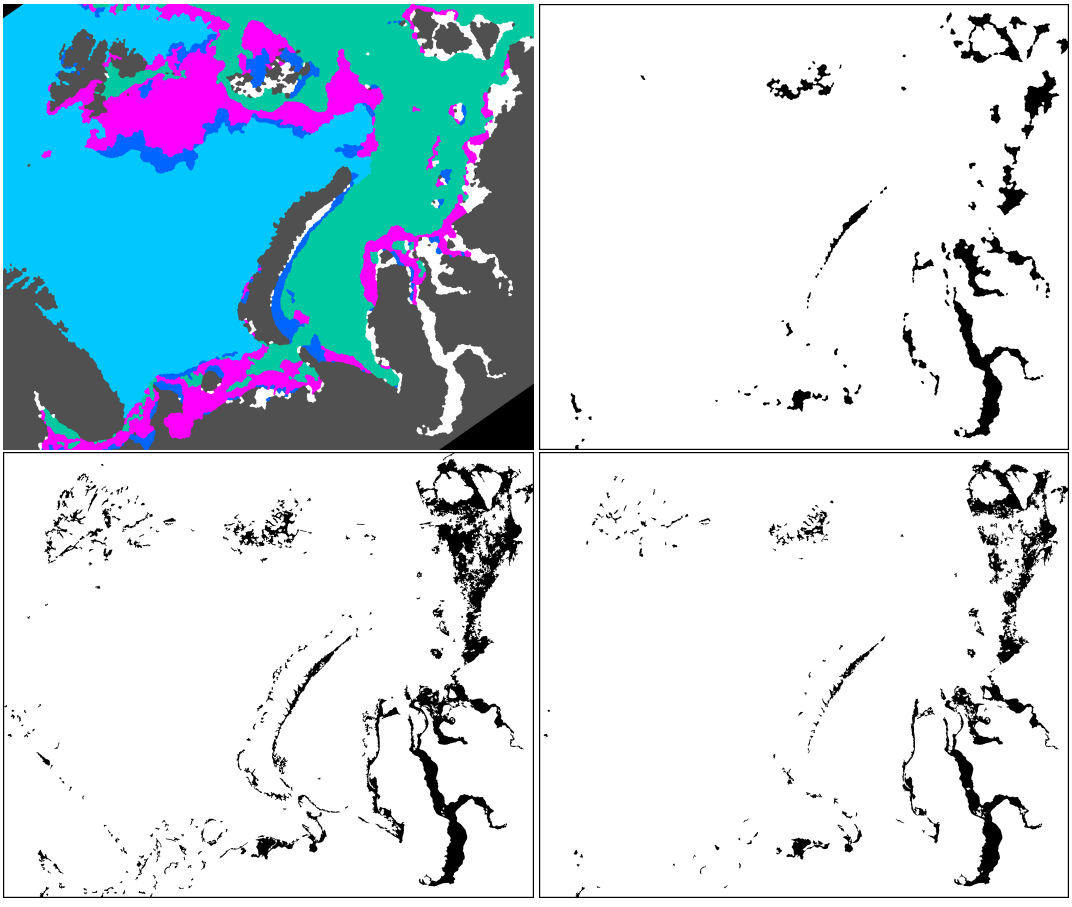

Figure 6. AARI ice chart of March 8, 2016, translated to the polar stereographic projection used in this study, LFI based on the AARI ice chart (black areas), LFI based on the FMI method, and LFI based on the FMI method with additional temporal filtering.

The Cryosphere Discuss., https://doi.org/10.5194/tc-2017-260
Manuscript under review for journal The Cryosphere
Discussion started: 5 December 2017
© Author(s) 2017. CC BY 4.0 License.

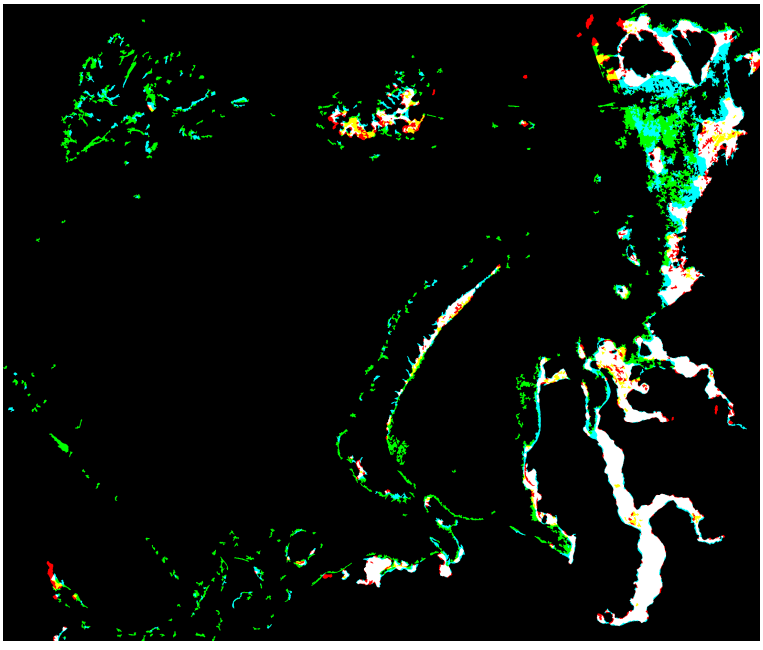

Figure 7. A false color image of March 8, 2016, combining the products in comparison. In the False color image Red=AARI LFI, Green=FMI-A LFI and Blue=FMI-B LFI. In the white areas all the three LFI estimates agree.

The Cryosphere Discuss., https://doi.org/10.5194/tc-2017-260
Manuscript under review for journal The Cryosphere
Discussion started: 5 December 2017
© Author(s) 2017. CC BY 4.0 License.

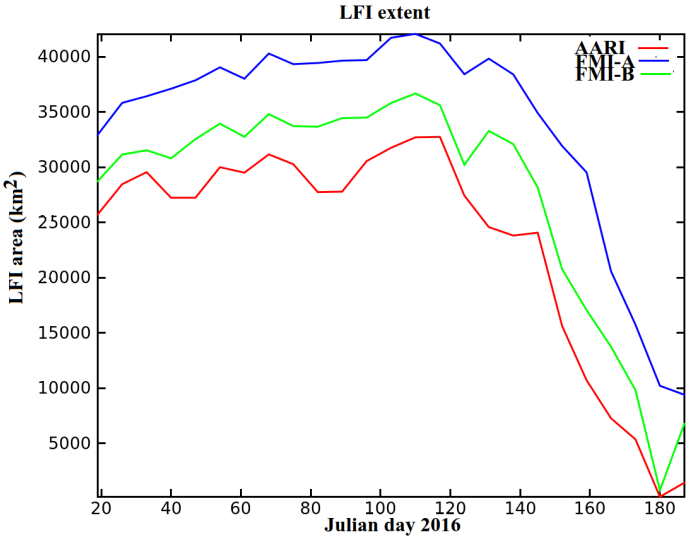

Figure 8. Time series of the weekly (from Nov 3 2015 until July 5 2016) LFI extent over the study according to FMI-A, FMI-B and AARI ice charts.

The Cryosphere Discuss., https://doi.org/10.5194/tc-2017-260
Manuscript under review for journal The Cryosphere
Discussion started: 5 December 2017
© Author(s) 2017. CC BY 4.0 License.

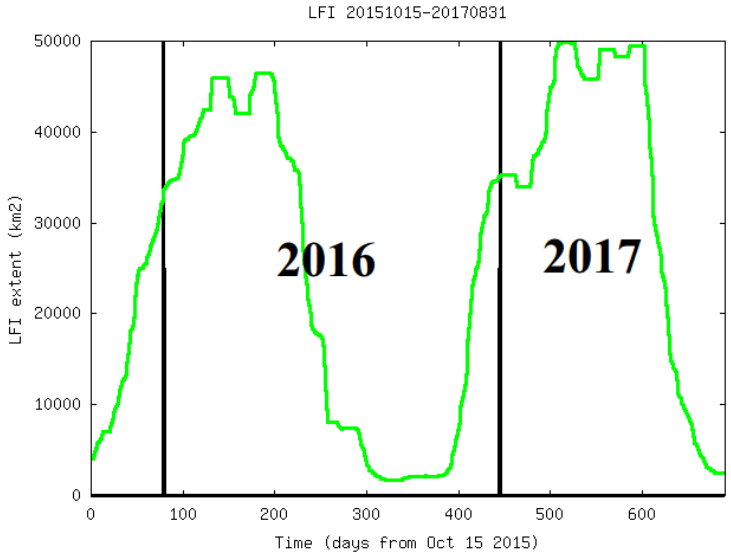

Figure 9. A LFI area times series of the whole study period from October 15 2015 to August 30 2017, using the FMI-B algorithm.